Analytical Biochemistry xxx (xxxx) xxx

Contents lists available at ScienceDirect

Analytical Biochemistry

journal homepage: www.elsevier.com/locate/yabio

Time-dependent influence of high glucose environment on the metabolism of neuronal immortalized cells

Laura Colombaioni [a], Beatrice Campanella [b,*], Riccardo Nieri [b], Massimo Onor [b], Edoardo Benedetti [c], Emilia Bramanti [b]

[a] Consiglio Nazionale delle Ricerche, Istituto di Neuroscienze, via Giuseppe Moruzzi 1, 56124, Pisa, Italy
[b] Consiglio Nazionale delle Ricerche, Istituto di Chimica dei Composti Organometallici, via Giuseppe Moruzzi 1, 56124, Pisa, Italy
[c] Unità di Ematologia, Dipartimento di Oncologia, Azienda Ospedaliero Universitaria Pisana, via Roma 67, 56100, Pisa, Italy

ARTICLE INFO

Keywords:
Targeted metabolomics
Hyperglycemia
Primary cultured hippocampal neurons
HPLC-DAD
Cell death
3-Way PCA

ABSTRACT

Mitochondria are organelles of bacterial origin historically identified as the cell power plant. In addition to energy, mitochondria produce reactive oxygen species and they have been found to have a key role in cell defense regulation, cell stress and damage. All the investigations regarding the nature of the molecules mediating these processes include compounds from mammalian cell metabolism. We hypothesize that the bacterial origin of mitochondria brings them to produce small fermentation products when cell is subjected to stress. In this work we studied the effect of hyperglycemia on the metabolome of hippocampal HN9.10e neurons, an *in vitro* model of one of the most vulnerable regions of central nervous system. Targeted metabolites were analyzed in the cell culture medium by liquid chromatography – diode array detection and headspace – gas chromatography – mass spectrometry. Twenty-two low molecular weight metabolites were identified and quantified in the growth medium of the cells, treated with 25, 50 or 75 mM glucose, sampled along 8 days to mimic a prolonged hyperglycemia. The results of statistical analysis showed the clear impairment of neuronal metabolism already after 48 h, represented by a significant reduction of the metabolic activity, together with the production of typical fermentative compounds.

1. Introduction

Glucose is the main energy source of our brain, but its excess strongly affects brain metabolism giving serious pathological consequences [1], Cerebral glucose metabolism is tightly linked to neuronal metabolism [2], likely because of the ATP-sensitive potassium (KATP) channels, which are found in many excitable cells, including cardiac myocytes, pancreatic β cells, and neurons [3,4].

Cho et al. found that high glucose induced apoptosis in SH-SY5Y neuronal cells via the mitochondria-dependent pathway due to the mitochondria oxidative phosphorylation, cell death regulation, and ROS production [5]. Macauley et al. reported that high glucose levels typical of type 2 diabetes alter both hippocampal interstitial fluid Aβ levels and neuronal activity in mice, acting as pharmacological manipulation of KATP channels in the hippocampus. KATP channel activation mediates the response of hippocampal neurons to hyperglycaemia by coupling metabolism with neuronal activity [6]. Elevated extracellular glucose levels can invoke indeed rapid changes in neuronal excitability through KATP channel closure and, thus, membrane depolarization [3].

Recent studies in primary cultured hippocampal neurons report that high glucose (from 50 up to 150 mM) up to 96 h is the main factor of diabetic cognitive impairment, and can cause hippocampus abnormalities due to reactive oxygen species (ROS) generation [7]. In their work Russell and co-workers indicate that 45 mM glucose levels induce in neurons ROS production, mitochondrial membrane depolarization, partial depletion of ATP, and activation of caspase-3 and -9 that precedes neuronal apoptosis [8]. Studies have demonstrated that hyperglycaemia arising from diabetes induces peripheral sensory neuronal impairment and mitochondrial dysfunction [9]. Furthermore, there is evidence that the hippocampal dysfunction in diabetic animals might result in cognitive deficits and increases the risk of depression and dementia [10].

It is known that in the central nervous system of many vertebrates, including humans, the neurogenesis continues during the adulthood.

* Corresponding author.
E-mail addresses: laura.colombaioni@in.cnr.it (L. Colombaioni), beatrice.campanella@cnr.it (B. Campanella), riccardonieri.nutrizionista@gmail.com (R. Nieri), massimo.onor@pi.iccom.cnr.it (M. Onor), edobenedetti@gmail.com (E. Benedetti), emilia.bramanti@pi.iccom.cnr.it (E. Bramanti).

https://doi.org/10.1016/j.ab.2022.114607
Received 7 October 2021; Received in revised form 7 February 2022; Accepted 17 February 2022
Available online 25 February 2022

This process has been well documented in neocortex, in striatum [11,12], and, in particular, in hippocampus [13]. The hippocampal neurogenesis is required for learning and memory processes [14,15], and it is also responsible for many different pathologies including mood disorders, stress and epilepsy [16,17]. Thus, the specific conditions able to influence the neurogenesis must be carefully addressed in the view that their deregulation could increase the risk of abnormalities in cognitive function.

Due to the role of hyperglycaemia in neurodegenerative diseases [18], and to the severe damage of hippocampal region in this kind of pathologies [19], the study of the effects of glucose in proliferating neurons is of crucial importance. By contrast, these cells are still largely uncharacterized from a metabolic point of view and the consequences of an elevated glucose exposure remain mostly unexplored. The effect of high-glucose environment on neuron metabolism was studied using nuclear magnetic resonance (NMR)-based metabolomics in primary neuron cultures to contribute to the understanding of the metabolic alterations and underlying pathogenesis of cognitive decline in diabetic patients [20].

Despite the analysis of cell culture medium (CCM) has several limitations, being limited to extracellular metabolites interchanged between cells and CCM (uptake of substrates/excretion), recent exometabolome studies of cell cultures have been reported [21–28]. The analysis of extracellular metabolites in CCM of living cells it allow to monitor the metabolic changes over time in the same cell culture, it guarantees a minimal sample handling of cells, it reflects the metabolic activity of cells in response to experimental perturbations without cell disruption. In several conditions (e.g. adherent cell lines) the CCM can be rapidly collected, diluted, filtered and analyzed, avoiding long and manifold extraction procedures (e.g. cell lysis).

Recently we have investigated the metabolic implications on the neuronal metabolism of HN9.10e cell line following a short and transient exposure to low thallium chloride doses, based on the chromatographic analysis of CCM and on morphological and functional tests [29,30]. The increased production of lactate and ethanol concentration was found to be associated with signs of cellular deregulation such as neurite shortening, loss of substrate adhesion, increase of cytoplasmic calcium, dose-dependent alteration of mitochondrial ROS (mtROS) level and of transmembrane mitochondrial potential ($\Delta\Psi m$) [30]. The exometabolomic profile of immortalized hippocampal neurons HN9.10e grown under standard conditions was also assessed by reversed phase liquid chromatography with diode array detector (RP-HPLC-DAD) method and by solid phase microextraction -head space -gas chromatography -mass spectrometry (SPME-HS-GCMS) for the study of volatile organic compounds (VOCs) [31].

In this work we studied the effect of glucose concentration in hippocampal HN9.10e neurons, a somatic fusion product of hippocampal cells from embryonic day 18 C57BL/6 mice and N18TG2 neuroblastoma cells [32]. This cell line shares many structural and functional features with primary hippocampal neurons and, consequently, it is a reliable *in vitro* model of one of the most vulnerable regions of central nervous system [33]. Since HN9.10e is a well-characterized cell line from the morphological and functional point of view, it allows a reliable evaluation of minute metabolic alterations, which is currently missing in the literature.

2. Materials and methods

2.1. Chemicals

Sulfuric acid for HPLC analysis was employed (30,743 Honeywell Fluka 95–97%). Methanol for RP-HPLC was purchased from Merck (34,860, ≥99.9%). Standard solutions for HPLC (TraceCERT, 1000 mg/L in water) and ethanol (analytical standard for GC) were purchased from Sigma Aldrich (Milan, Italy). All compounds had purity higher than 98% and, thus, were used without any further purification. Analytes stock solutions were prepared by dissolving a weighed amount of the pure compound in deionized water (MilliQ; 18.2 MΩ cm^{-1} at 25 °C, Millipore, Bedford, MA, USA) and stored at 4 °C up to 1 month in an amber vial.

Solid Phase Micro-Extraction Fiber based on 85 μm carboxen/polydimethylsiloxane (CAR/PDMS) were employed for the preconcentration of ethanol in the HS.

Helium 5.6 IP was purchased from Sol Group Spa (Italy) and was further purified with a super clean filter purchased from Agilent Technologies (USA) to remove water, oxygen and hydrocarbon contaminants.

2.2. Cell culture of HN9.10e neuroblasts

Immortalized hippocampal neurons HN9.10e were a kind gift of Dr. Kieran Breen, Ninewells Hospital, Dundee, UK [34]. HN9.10e cells were grown in DMEM-F12 (1:1) medium HEPES buffered, supplemented with 4 mM L-glutamine, 50 UI/mL penicillin and 50 mg/mL streptomycin, at 37 °C in humidified atmosphere containing 5% CO_2. Cells, seeded at 20,000 cell/cm^2 in culture flasks containing 5 mL of medium, were left in culture for 4 days before treatments to allow substrate adhesion and grown to an optimal 40% confluence. After this, they were incubated in CCM containing 25, 50 or 75 mM glucose. To take account of variations, two independent batches of cells were cultured for each glucose level.

The experimental design adopted as well as the names for the samples analyzed in this study are shown in Supplementary Table S1. To investigate the effects of high glucose culture medium, the HN9.10e hippocampal neuroblasts were incubated with three different doses of glucose representing a 2 and 3-fold increase from baseline (25 mM glucose). After 48 h of culturing in the basal condition (glucose 25 mM, g25_Tx, with x = 0, 1, 2, 3, 4, 5 and 6 for t = 0 h, 48 h, 96 h, 120 h, 144 h, 168 h and 192 h, respectively), glucose was kept 25 mM in cell culture medium (CCM) of control cultures and increased to 50 (g50_Tx), and 75 mM (g75_Tx). Two independent cell cultures for each glucose level were grown. CCM containing the established glucose concentration was collected and refreshed after the first 48 h and successively every 24 h up to 192 h (8 days) after the beginning of the experiment.

2.3. Automated imaging of HN9.10e neuroblasts

Cell morphology and growth rate avoiding the metabolic alterations were investigated using an inverted microscope (Axiovert 35, Carl Zeiss, Oberkochen, Germany) equipped with Nomarski interference contrast optics and 40x or 63x objectives that allowed to enhance the contrast of unstained neurons in the cultures. This set up allowed us to monitor growth and death events in unstained neuron cultures, without the need for any dye or fluorescent probes. The neuronal staining would imply indeed a long permanence of dyes in CCM, due to the extended sampling and monitoring time (192 h). However, this could induce unpredictable metabolic alterations, or even a certain degree of vitality loss.

The degree of cell confluence was evaluated by the automated measure of the ratio [surface occupied by cells/cell-free surface] obtained after the cell boundaries were determined with the standard function “Edge Detection” of the MATLAB scientific software (The MathWorks, Massachusetts, U.S.A.), adapted to the specific contrast level and cell shapes of HN9.10e cultures. The measurements have been performed in $n = 5$ independent, non-overlapping, fields (400 × 400 μm) for each dose of glucose and sampling time. In the initial condition (T0), at a confluence value 0.4, each field contained, on average, 150 cells. The HN9.10e cell line (embryonic hippocampal neurons), developed by Lee H.J. et al., was a kind gift of Dr. Kieran C. Breen, Ninewells Hospital & Medical School, Dundee DD1 9SY, UK.

2.4. Experiments to exclude an artifactual origin of CCM exo-metabolites

To rule out a possible artifactual origin of specific extracellular

metabolites in CCM (such as ethanol and butyric acid, BA) several control experiments were performed in different conditions. First, cell-free CCM was incubated in sealed flasks (N = 3) at 37 °C for various times, up to 25 days. Neither ethanol nor BA were detected in this experimental condition, excluding that they may originate from CCM degradation. Furthermore, to obtain strong evidence that HN9.10e cultures are sterile and free from even the slightest bacterial contamination, 500 μL of CCM from every experimental flask showing an increased concentration of ethanol and/or BA were added to control flasks containing 5 mL of fresh medium and incubated at 37 °C up to 25 days. Over such long times, any minimal bacterial contamination would amplify and become evident. However, neither bacterial growth, nor ethanol and BA were detected in the control flasks, excluding a bacterial origin of these compounds.

All details on targeted metabolomics, data processing and statistical analysis have been reported in the Supplementary Material, which includes Tables S2A, S2B and S2C.

3. Results

3.1. Glucose influences the growth rate and viability of HN9.10e neuroblasts

The effects of glucose on the neuronal growth were evaluated as confluence fraction of the cell population, whose values are reported in Fig. 1A and in Supplementary Table S1.

In 25 mM glucose cell, confluence (Fig. 1A) increased linearly with time up to 192 h (T6). In hyperglycemic conditions (50 and 75 mM) a higher growth rate, compared to the basal condition (25 mM), was observed, as shown by the slope of the confluence fraction curve during the first 96 h of treatment (T0-T2). Starting from 120 h (T3) the growth rate (i.e. the first derivative of the curves shown in Fig. 1A) in glucose 50 and 75 mM decreased. In cultures treated with 75 mM glucose the cell confluence decreased abruptly and significantly at 192 h (T6). Thus, early hyperglycemia increased the rate of cell proliferation; later (observed in our experiments only for 75 mM hyperglycemia, and even

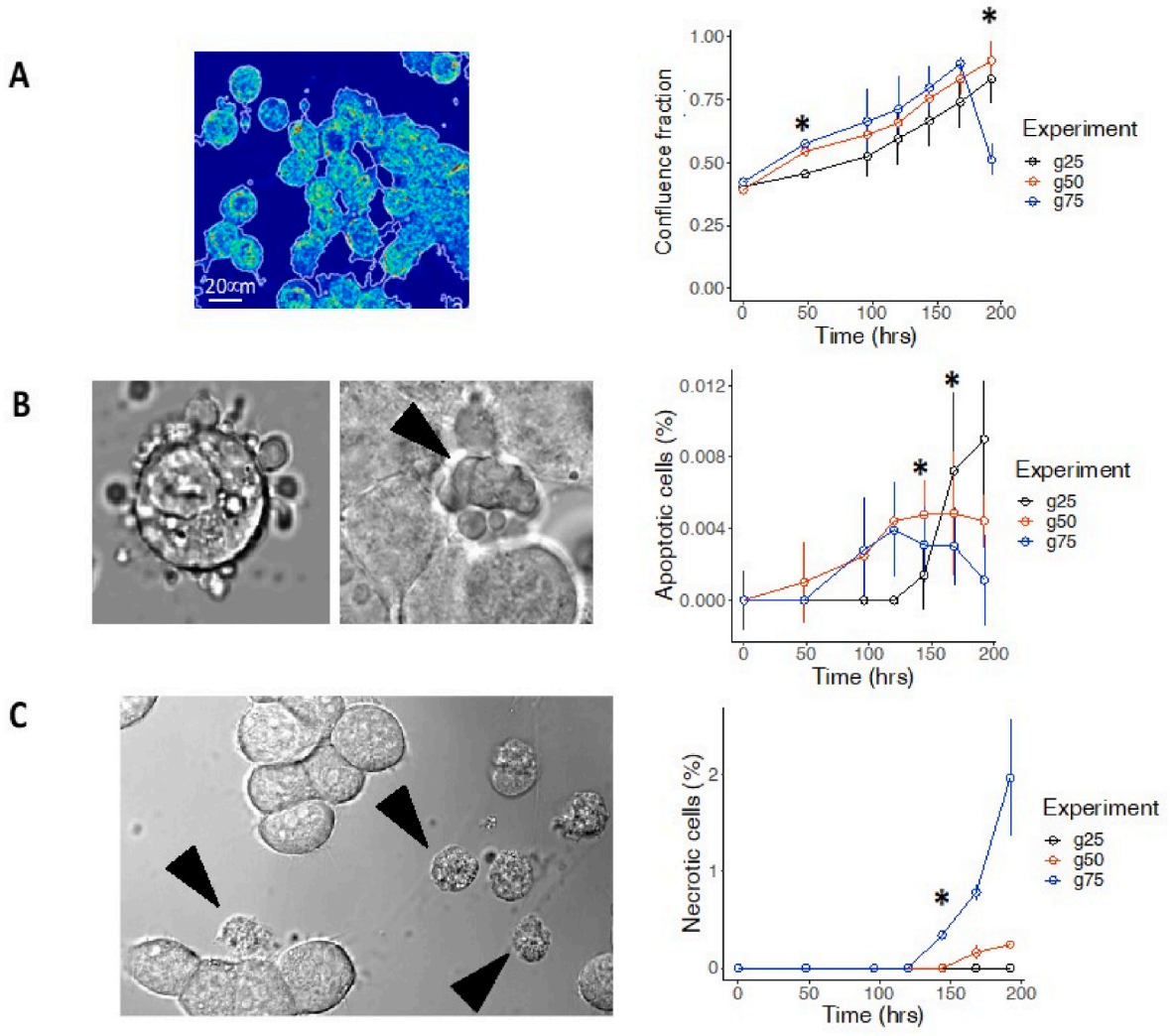

Fig. 1. Effect of glucose on growth rate and viability. A) Left panel: a representative image illustrates the typical cell contouring by the Matlab scientific software. The ratio [surface occupied by cells/cell-free surface] is used to quantify cell density and growth rate in cultures incubated with 25, 50, 75 mM glucose. Right panels: the cell confluence fraction for the different glucose concentrations. Each value represents the mean of the ratio [surface occupied by cells/total surface] measured in $n = 5$ independent, non-overlapping fields 400 x400 μm. **B**) Representative images of apoptotic HN9.10e neuroblasts in early (left panel) or late phase (middle panel), arrow indicates a typical collapsed and fragmented nucleus. Right panel: apoptosis percentage for the different glucose concentrations. **C**) Left panel: typical necrotic morphology: arrows point to HN9.10e neuroblasts dying for necrosis. Right panel: necrosis percentage for the different glucose concentrations. Raw data of confluence, apoptotic and necrotic cells are reported in Supplementary Table S1. Apoptotic and necrotic cells were counted in the same fields in which confluence was quantified. Stars indicate a p-value < 0.05 for one-way ANOVA comparison.

later likely for experiments in 50 mM glucose) gave a drop in cell vitality suggesting an enhanced cellular vulnerability in high glucose conditions.

To investigate the role of cell death in this process, we performed a specific analysis of the apoptosis and necrosis percentage in the different experimental conditions. Apoptotic and necrotic cells were distinguished on the basis of their standard, well recognized, morphological features [35]. The early phase of apoptosis is characterized by blebbing of the plasma membrane without integrity loss, followed by cytoplasmic shrinkage, nuclear collapse, and formation of pyknotic bodies of condensed chromatin (Fig. 1 B left and middle panel). Necrotic cells exhibit loss of membrane integrity and disaggregated appearance in transmitted light microscopy (Fig. 1C left panel).

The apoptosis percentage was very low in each experimental group (<0.01%) (Fig. 1B, right panel). A minimal apoptosis incidence is a physiological phenomenon, corresponding to the normal cellular turnover of the culture. In 25 mM glucose the apoptosis percentage linearly increased indeed with the confluence, and it typically reached the 0.01% value for a 95–98% confluence. During the first 6 days (T0-T4), the apoptosis percentage in cells treated with 50 and 75 mM glucose was anyway higher compared to cells in control condition (25 mM). At T5-T6 the percentage of apoptotic cells in 25 mM glucose was higher than in hyperglycemic conditions: at T5 0.005% in 50 mM, 0.003% in 75 mM compared to 0.007% in 25 mM glucose (4% relative standard deviation; $p < 0.001$). Thus, in hyperglycemic conditions neuronal energetics was still able to support the active process of apoptotic death, but especially in 75 mM glucose at T6 apoptosis showed a drop and a rise of necrotic cells.

In parallel, the necrotic death, undetectable in any experimental group until day 5 (T3), increased considerably in 50 and 75 mM glucose beyond this time limit (Fig. 1C, right panel). The raise was gradual in 50 mM, exponential in 75 mM glucose, partially responsible for the sharp drop of the cell confluence value at T6.

Based on these functional and morphological observations on the cultures of HN9.10e living cells, we performed the exometabolome screening in the CCM at the corresponding times.

3.2. Principal components analysis (PCA)

SPME-HS-GCMS and RP-HPLC-DAD methods were then applied for targeted metabolomic analysis. Fig. 2(A) and (B) show representative HS-SPME-GC-MS and HPLC-UV (220 nm), respectively, of CCM after neuron culturing in 25 mM glucose at T0, 50 and 75 mM glucose at T1.

Mean concentration and standard deviation of the 22 quantified

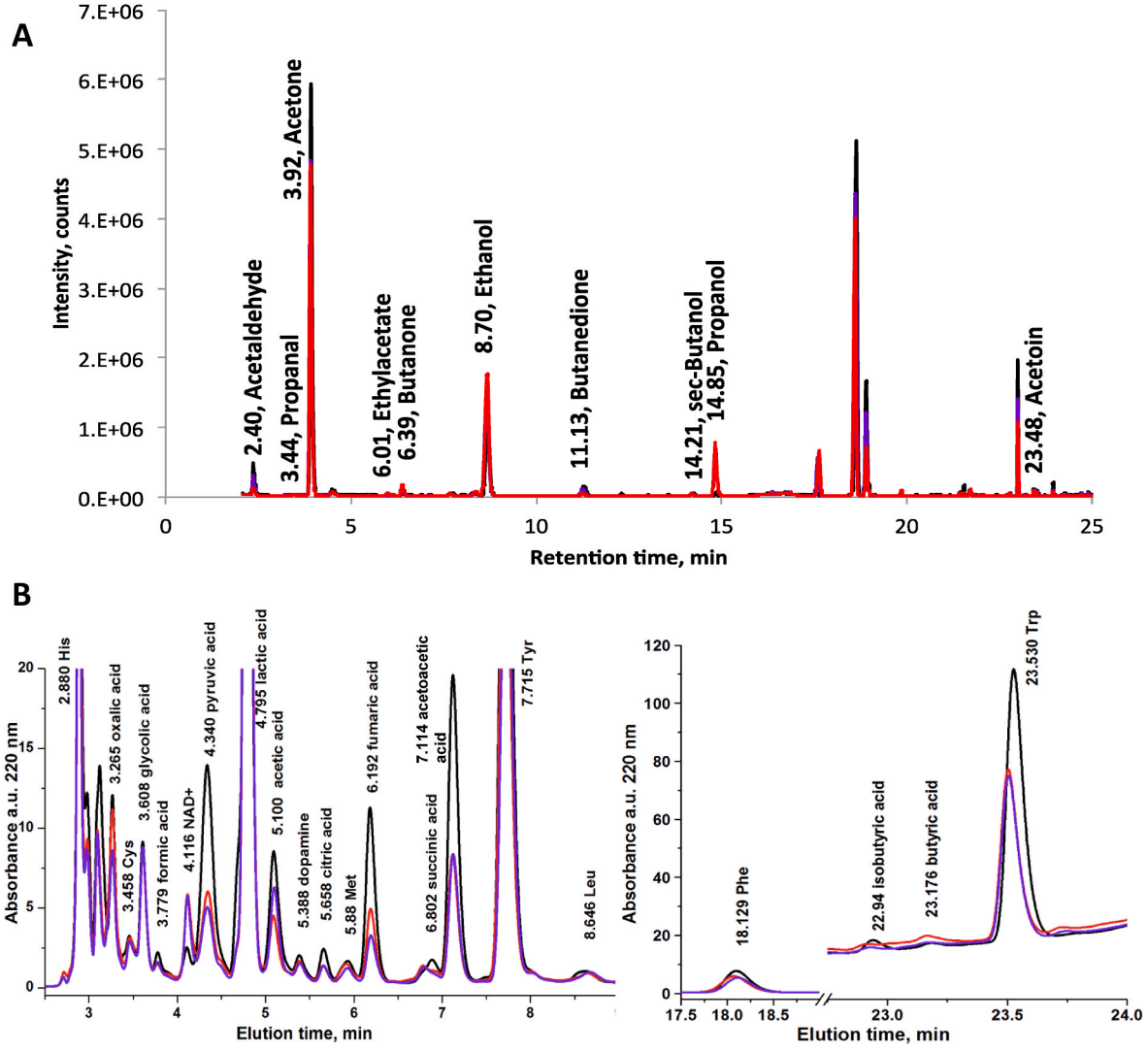

Fig. 2. A) Representative total ion SPME-HS-GC-MS chromatograms and B) HPLC-UV chromatograms at 220 nm, respectively, of CCM after neuron culturing in 25 mM glucose at T0 (black line), 50 at T1 (purple line) and 75 mM glucose at T1 (red line). (For interpretation of the references to colour in this figure legend, the reader is referred to the Web version of this article.)

metabolites are reported in Supplementary Table S3.

For statistical comparison, samples were divided in two sub-groups (i.e. basal at T0, all grown in 25 mM glucose, versus CCM samples at 48 h, and CCM sampled from 48 h to 168 h). The sampling point at 192 h (T6) was excluded from the analysis as the drop of cell confluency values suggests the massive release of metabolites due to cell necrosis. Data related to PCA scores and loadings are reported in Supplementary Tables S4 and S5, respectively.

First, we compare samples at T0 (gx_T0, see Table S1) with samples at T1 = 48 h (gx_T1, see Table S1). All gx_T0 samples grown in 25 mM glucose represent the reference basal condition, while gx_T1 (x = 25, 50 or 75) samples had experienced equal or increasing glucose quantities. Fig. 3 shows the PCA that showed a good separation along Dim1 (which accounts for 76.5% of total variance) between cells grown in 25 mM glucose with respect to those treated with 50 mM and 75 mM glucose. The second dimension (12.5% of total variance) differentiated samples treated with 50 mM glucose from those treated with 75 mM glucose, while cells grown in 25 mM glucose and collected after 48 h (g25_T1) clusterized with the respective basal (g25_T0). The analysis of the loading plot showed that the three basal samples and g25_T1 are strongly positively correlated with all the metabolites, except for oxidized nicotinamide adenine dinucleotide (NAD^+) (which is responsible for the separation of g50_T1), butyric acid and ethanol (both correlated with g75_T1).

PCA was also used to represent samples from gx_T1 to gx_T5 (x = 25, 50 or 75 mM), representing the temporal evolution of the three classes of experiments at increasing glucose concentrations. Fig. 4 shows a clear separation through the second dimension of all g75 samples with respect to the others, while a weaker distinction appears along the first PC for g25 and g50 samples. The latter seems more influenced by the temporal evolution, the samples moving from right to left with increasing time, i.e. for increasing time of permanence of cells in the corresponding medium. The loading plot mostly reflects the same plot obtained in the previous PCA. Here, the metabolites belonging to the TCA cycle (succinic acid, fumaric acid, propionic and citric acid) are positively correlated among them and with the samples at 25 mM glucose analyzed after 48 (T1) and 96 h (T2), on the right side of score plot. With respect to the results of the PCA reported in Figs. 3 and 4, here ethanol is strongly correlated with NAD^+ and with the samples treated with 50 mM glucose. The hypothesis emerging from this analysis is that a high glucose concentration (i.e. 75 mM) induces a switching of HN9.10e neurons metabolism toward alternative metabolic pathways involving, in the case investigated, the production of butyric acid. At lower glucose concentrations (i.e. 50 mM) an alteration of metabolic pathways typical of normo-glycemic conditions likely occurs.

3.3. Three-way principal component analysis (3- way PCA)

PCA is generally not recommended to handle time-course data, since they are non-independent. Here, PCA was used to have an overview of the quality of the acquired data. However, considering that in our case the same analyses have been performed on the same cell cultures on different days, a third mode needs to be added to decompose metabolomic variations derived from time to those derived from glucose treatment. A 3-way PCA by applying the Tucker 3 model was then performed, which is particularly suitable for the management of three-dimensional data, especially when samples are analyzed over time. For a more complete treatment of this subject the reader should refer to [36].

Our data set can be represented as a parallelepiped of size I x J x K, where I is the number of tested glucose concentrations (objects, I = 3), J is the number of metabolites (variables, J = 22) and K is the number of sampling times (conditions, K = 5). The final results of 3-way PCA are three sets of loadings, which from a graphical point of view closely follow the score plot of standard PCA and whose relationship is described by a core array. Two principal components for each mode (i.e. samples, variables and times) were retained, thus the final array is a cube having dimension [2,2,2]. The total variance explained by the Tucker model is 69.4%, which is fully satisfying considering the variability of biological systems. After body diagonalization, the following core array is obtained:

$$\begin{bmatrix} g_{111} & g_{121} & g_{112} & g_{122} \\ g_{211} & g_{221} & g_{212} & g_{222} \end{bmatrix}$$

$$\begin{bmatrix} 15.542 & 2.1486 & -0.21391 & -1.9009 \\ 0.76987 & 0.31494 & -5.1932 & -6.5705 \end{bmatrix}$$

Despite the matrix does not show a super-diagonal structure, the element $g_{1,1,1}$ is by far the largest one, followed by the element $g_{2,2,2}$. This behaviour permits to display the three loading plots in a single triplot (Fig. 5, analogously to PCA biplot) for the joint interpretation of the first two components for each mode.

From Fig. 5, it can be noted that the points representing each sampling time (T1-T5) are elongated on Axis 1 and that the distance between

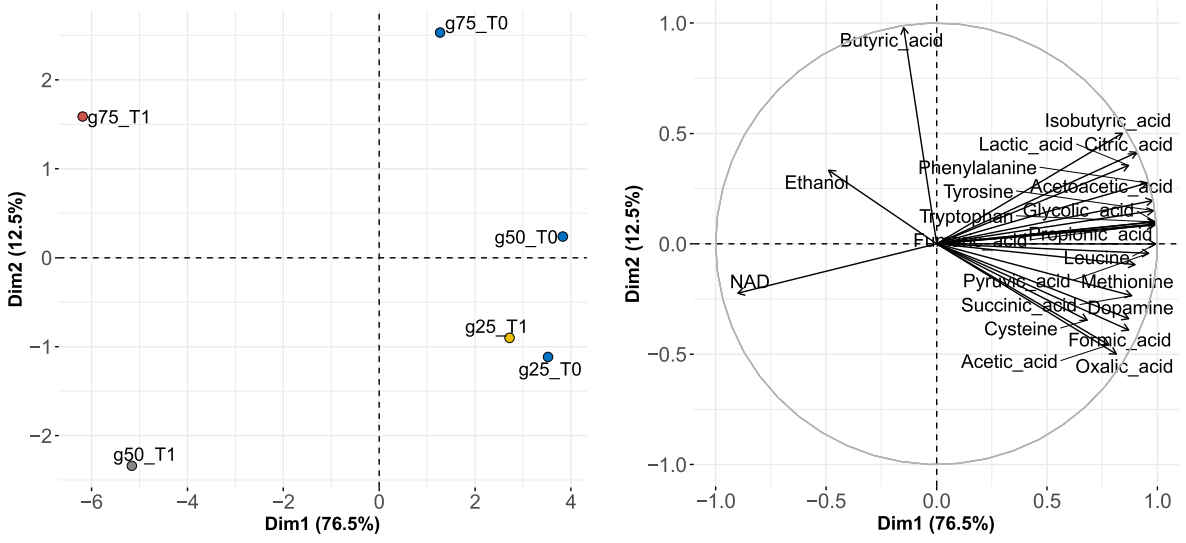

Fig. 3. Principal component 1 (Dim1) versus principal component 2 (Dim2) score and loading plot based on the result of principal component analysis performed for T0 and T1 samples (basal: blue; 25 mM glucose: yellow; 50 mM glucose: grey; 75 mM glucose: red). Percentage in the axis indicates the fraction of variance explained by each principal component.

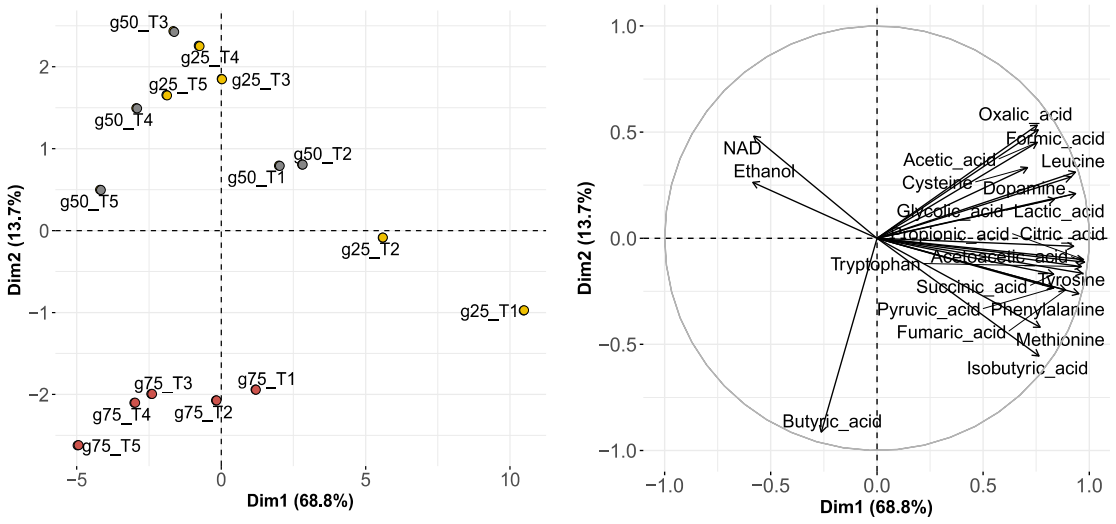

Fig. 4. Principal component 1 (Dim1) versus principal component 2 (Dim2) score and loading plot based on the result of principal component analysis performed for samples from T1 to T5 (25 mM glucose: yellow; 50 mM glucose: grey; 75 mM glucose: red). Percentage in the axis indicates the fraction of variance explained by each principal component.

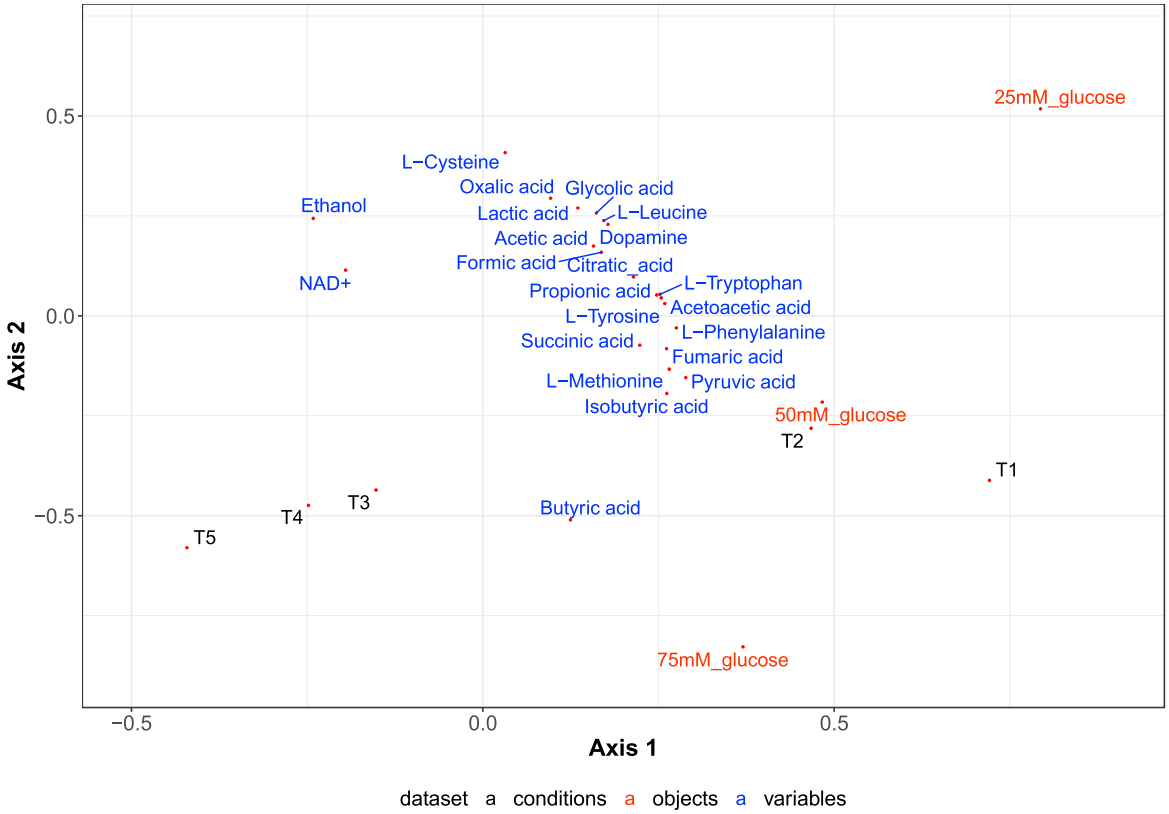

Fig. 5. Triplot resulting from 3-way PCA applied to the T1-T5 dataset (conditions = sampling times; objects = glucose concentration; variables = metabolites). The evolution of each metabolic perturbation over time is directly interpretable from time loading.

the five points is not equal, similarly to the score plot of PCA. Three clusters can be identified as T1, T2 and T3-T4-T5. A possible interpretation is that the kinetics of the metabolic changes due to glucose treatment is not constant for each time lapse.

The points related to glucose treatment (25 mM glucose, 50 mM glucose and 75 mM glucose) are spread along Axis 2, with the conditions at higher glucose concentration (50 and 75 mM) more closely related between them with respect to the control at 25 mM. It must be noticed

that 3-way PCA could detect the glucose effect much more efficiently than standard PCA.

Most of the variables are influenced neither by time along Axis 1 nor by glucose concentration along Axis 2 (their coordinates in the PC space are almost zero), with the exception of butyric acid and L-cysteine which appear oppositely correlated along Axis 2 (butyric acid is correlated with high glucose while L-cysteine is correlated with low glucose), and NAD^+ and ethanol, whose loadings are higher for Axis 1, i.e. they became significant for longer treatments (T3-T5) with 50 mM glucose.

Two-way mixed ANOVA was used to evaluate the interaction between glucose treatment (i.e., the between-subjects factor) and time (i.e., the within-subjects factor) in explaining the extracellular metabolites release. Fig. 6 shows the time dependent box plots of NAD^+ and butyric acid together with the results of pairwise comparisons following two-way mixed ANOVA analysis, which resulted in a significant factors interaction. The same plot is reported for all cases in Supplementary Information (Fig. S1) where a statistically significant interaction between glucose treatment and time was detected.

4. Discussion

The effects of a high glucose environment on metabolome have been reported for cell lines from pancreas (BRIN-BD11 and INS-1E) [37], liver (HepG2) [38], and kidneys (HK-2) [39–41]. In the studies mentioned, 25 mM was the maximum concentration of glucose employed to treat the cells, with respect to a physiological glucose concentration in the plasma equal to 5.5 mM [42].

Due to the serious neurological complications associated with

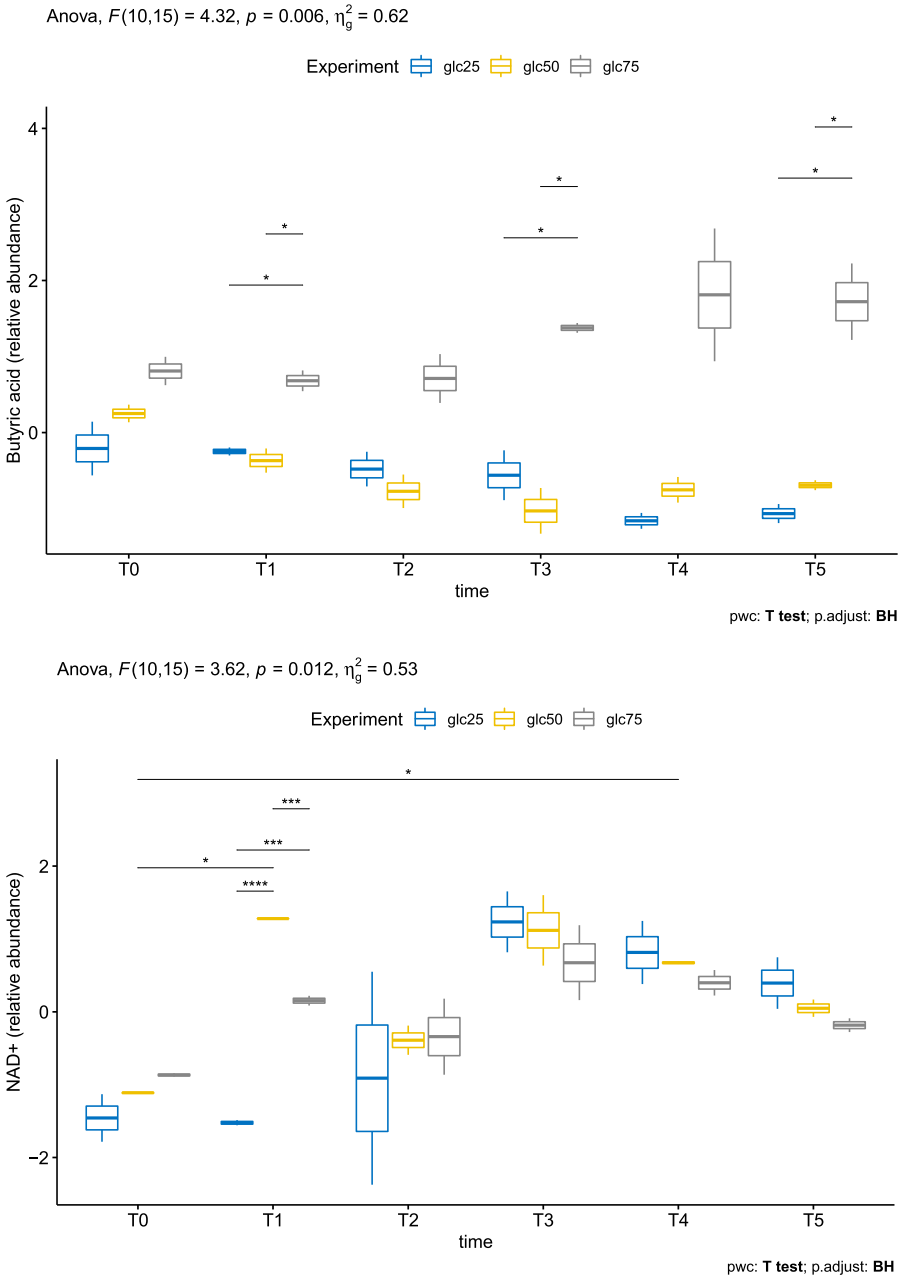

Fig. 6. Box plots of butyric acid and NAD^+ for each glucose concentration (g25, g50 and g75) and sampling time. The result of two-way mixed ANOVA for factors interaction is reported on the top of each graph. Stars are related to the result of pairwise comparisons p-values (*p ≤ 0.05; **p ≤ 0.01; ***p ≤ 0.001; ****p ≤ 0.0001).

pathologies as diabetes, we propose here the HN9.10e hippocampal neuroblasts as model line to study hyperglycaemia metabolic effects. The experimental conditions here adopted do not allow HN9.10e neuroblast differentiation since, due to the frequent change of CCM, the endogenously produced neurotrophins and growth factors cannot reach the optimal concentration required to trigger the differentiation process. Hence the cultures, remaining undifferentiated, represent a reliable *in vitro* model of proliferating hippocampal neuroblasts. The choice of examining the exometabolome instead of cell lysates is due to the relative simplicity of measuring over time and in the same cultured cells the variations of chemical composition in CCM, which rapidly provides the response of cells to external stimuli with a minimal perturbation of cell system [22,24,28].

Adherent neuronal cells are usually grown in the Dulbecco's Modified Eagle Medium (DMEM) containing 25 mM glucose, which in most of the studies dealing with neuroblasts represents a consolidated basal condition, because of the high metabolic rates of neuroblasts [43]. The high energy demand in neurons results from their neurotransmitter functions linked with continuous depolarization/repolarization cycles of 5–50 Hz frequency. The maintenance of this basal neuronal function, especially in culture neurons, requires marked energy expenses for the restoration of membrane potential [44]. Liu et al. verified that the osmolality of glucose solutions between 25 and 150 mM being between 260 and 320 mOsm/kg, did not exert any effect on cell normal metabolism [7].

In this work in addition to the basal concentration of 25 mM glucose, we investigated the effects of 50 mM and 75 mM glucose, to study the occurrence of an eventual cellular metabolic shift.

We found that the cell viability in HN9.10e cells exposed to 75 mM glucose decreased remarkably after 8 days, compared to basal group, in agreement with previous studies [7]. Differential interference contrast microscopy evidenced that the sharp drop of cell viability of g75_T6 group is due to a massive necrosis process, suggesting that long-term exposure to high glucose concentrations could impair the mitochondrial function [7–9,45]. Other forms of cell death, such as necroptosis triggered by inflammation, induced by hyperglycemia, cannot be excluded [46–48].

Multivariate analysis and detailed metabolite level measurement showed that the treatment with high doses of glucose induced a decrease of the concentration of several metabolites of TCA cycle, which despite being intracellular intermediates were found in the CCM. A reasonable hypothesis is the release of these metabolites in the extra-cellular medium by means of the monocarboxylate (MCTs), di- and tri-carboxylate transporters [49,50].

The results obtained from 3-way PCA, which is a statistical technique suitable for the analysis of time-series, confirmed that neuronal cells have dose-dependent characteristic metabolic features, depending on glucose concentration level. This observation is in agreement with the results found in glucose-stimulated HK-2 cell by Wei et al. [41], which correlated the increase of glycolysis and glucose oxidation with characteristic metabolic changes, including the increase of lactate-to-pyruvate ratio and the suppression of TCA cycle.

In HN9.10e hippocampal neuroblasts exposed to moderately high glucose levels (i.e. 50 mM) ethanol production was strongly stimulated with respect to basal condition, and NAD^+ levels increased, but the levels of these metabolites seemed more related to exposure time rather than to the glucose level in CCM. The delay in the ethanol production agrees with our previous observation [29], and it could be related to an ancestral "safety procedure" [51], which allows the cells to proliferate also when lactate concentration increases because mitochondrial function is effectively or apparently compromised [52] or in hypoxic environments, recovering the energy for cell survival converting lactate in ethanol [53,54]. It is known that the mitochondrial pyruvate decarboxylase (EC 4.1.1.1, a thiamine pyrophosphate and magnesium-dependent enzyme) and the cytosolic ADH permits in some species of fish (including goldfish and carp) to perform ethanol fermentation (along with lactic acid fermentation) when oxygen is scarce [55]. The activity of ADH is at least 100-fold higher than that of pyruvate decarboxylase. In this way the acetaldehyde produced by pyruvate decarboxylase is not accumulated because it is fast converted into ethanol [55]. In neuronal cells ADH is not expressed and the enzymes involved in ethanol/acetaldehyde conversion are catalase and Cytochrome P450 2E1 (CYP2E1), which belongs to P450 family [56]. These enzymes are typically involved in ethanol detoxification [57]. It cannot be excluded that one or both these enzymes may work also to produce ethanol as previously reported [29].

The increase of NAD^+ is consistent with its recognized role in neuronal survival, mitochondrial function, metabolism and ageing, and in the activation of a salvage pathway in neurons [58–62]. The increase of glycolysis enhances, as well, NADH oxidation to NAD^+, inducing an adaptive shift in energy metabolism [63].

The most outbreaking result obtained in this work is the detection of high levels of butyric acid (BA), which was the main metabolite increasing after treatment with 50 and 75 mM glucose (Fig. 6). Butyrate is produced by several fermentation processes of obligate anaerobic bacteria with the production of 3 molecules of ATP for each glucose molecule. Other pathways to butyrate include succinate reduction and crotonate disproportionation. It is universally accepted that mammalian cells do not produce butyrate. In humans the only significant sources of butyrate are the gut microbiota and the ingestion of dairy products. It is known, as well, that the treatment of neurons with BA and its derivates (e.g. gamma-amino butyric acid, GABA or drugs) gives significant metabolic alterations (oxidative stress, altered calcium homeostasis, neurite retraction, apoptosis) according to the recent findings related to the so called *gut-brain axis* [64–67]. All these results refer to the effects of *exogenous* BA, i.e. BA administered to cell cultures or produced by intestinal bacteria.

The increase of BA found in this work is related to the endogenous production of BA by HN9.10e neurons metabolism. Currently, we have no proven explanations on the mechanism or mechanisms that were involved in the production of BA by primary hippocampal neurons. This issue requires further investigation. We might hypothesize that this increase is related to the balance in neurons between pentose phosphate pathway (PPP) and glycolysis. Once trapped in cells as glucose-6-phosphate, glucose may go through glycolysis, PPP or it can be employed for the glycogen synthesis [68]. However, neurons are not able to synthesize glycogen [69,70], thus, glucose trapped in neurons as glucose-6-phosphate is mainly processed through the oxidative branch of the PPP. This pathway is the main producer of reducing equivalents in the form of NADPH. In normoglycemic conditions NADPH is used to regenerate reduced glutathione, which is the main ROS scavenging agent in neurons and it is employed, in less extent, to synthesize fatty acids.

In the early stage of hyperglycemic conditions, glycolysis is pushed by excess substrate, and neurons undergo oxidative stress with a high production of ROS [7]. Later, hyperglycaemia likely induces a metabolic reprogramming in a "Warburg-like" phenotype, switching from oxidative phosphorylation to glycolysis, TCA cycle suppression, and redirecting glucose as glucose-6-phosphate through the PPP as "safety procedure" to increase NADPH production [71]. The linear decrease of TCA cycle metabolites concentration over the time at the three glucose doses (Fig. S1), confirms the metabolic switch. This metabolic reprogramming is found in several diseases related to oxidative stress, likely triggered by mitochondrial dysfunction and massive ROS production [71].

The excess of glucose-6-phosphate and the consequent high consumption of NADPH in the first steps might avoid the elongation of short fatty acids. The hypothetical inhibition of the elongation steps could bring to BA release from butyryl-ACP by a thioesterase enzyme. As BA is well known to modulate gene expression due to its action as a histone deacetylase [72,73], and it is responsible for neuronal damage observed in short-chain acyl-CoA dehydrogenase deficiency (SCADD) [71], high

concentration levels of BA may be responsible for oxidative damage and mitochondrial dysfunction and massive cell death observed at 192 h.

Considering the bacterial origin of mitochondria [74], it can be hypothesized that any response of cell to stress agents that involve an alteration of energetic metabolism (high glucose concentration in this study, thallium contamination investigated in previous ones [29,30]) recalls ancestor mechanisms to preserve cell vitality.

Fig. 7 shows potential pathways that involve the metabolites determined in HN9.10e cell lines and that significantly increases or decreases their extracellular concentration, assuming specific or aspecific transport outside the cells. Figs. 6 and S3 show the enlargement of the time dependent plots of some key metabolites for an easier inspection.

L-Tyrosine, L-Phenylalanine and L-Tryptophan are precursor of L-Glutamic Acid, the main excitatory neurotransmitter of the mammal brain [75], dopamine, a monoamine neurotransmitters involved in the stability of hippocampus-dependent memory [81], and several neuroactive compounds (such as 5-hydroxytryptamine, kynurenines and melatonin) [82,83], respectively. Neutral, branched L-Leucine is known to be involved in the neuronal signaling process [76], and in the in regulation of glutamate levels [84]. Lactic acid, the main metabolite of CCM after cell culturing, may derive from glucose and L-Glutamine metabolism [77]. Glycolic or hydroxy acetic acid derives from gastrointestinal yeast overgrowth, bacterial species or dietary sources containing glycerol [78]. However, in eukaryotic cells glycolic acid could arise from L-Glycine and glyoxylate metabolism through glyoxalases [78–80]. In addition to glycolate, intermediate glyoxylate can be metabolized to formate and oxalate and CO_2 [78]. Acetoacetate is one of the main ketone bodies produced during ketogenesis. Its high concentration in CCM, as well as the high concentration of acetic acid, is suggestive of an excess of acetyl-CoA and it should protect against oxidative glutamate toxicity [85,86].

HS-SPME-GC-MS data are reported in Table S3. With the exception of ethanol, any variations detected in VOCs levels could not be related to the treatment with glucose but rather to cell ageing.

5. Conclusions

The number of metabolomics studies applied to cell-cultures is still low if reported to the plenty of existing literature on animal models or human body fluids [27], and the available data in this area are often fragmented. Although Seahorse analysis [87] and other specific assays to determine ROS, Ca^{++} release and the mitochondrial potential will complement this study, the results herein reported represent a tile in the exploration of cell metabolome, aiming to clarify with a simple targeted approach the unbalances deriving from high-glucose environments in HN9.10e immortalized neurons.

This work allowed us to find two main metabolites that increase in HN9.10e cultured immortalized cell line in hyperglycemic conditions: NAD^+ and butyric acid. These two molecules are known to act as signaling molecules and suggest (i) a hyperglycemia-induced switch of neuronal metabolism toward glycolytic pathway as energetic source and toward pentose phosphate pathway as "safety procedure" to increase NADPH production; (ii) an "attempt" of fatty acid synthesis due to the excess of acetyl-CoA. The metabolic alteration is evidenced only by a sudden, massive cell death classified as necrosis after 192 h, which reflects serious mitochondrial damage due to ROS accumulation, in agreement with previous metabolomic studies on the effects of glucose on different cell lines from hippocampus.

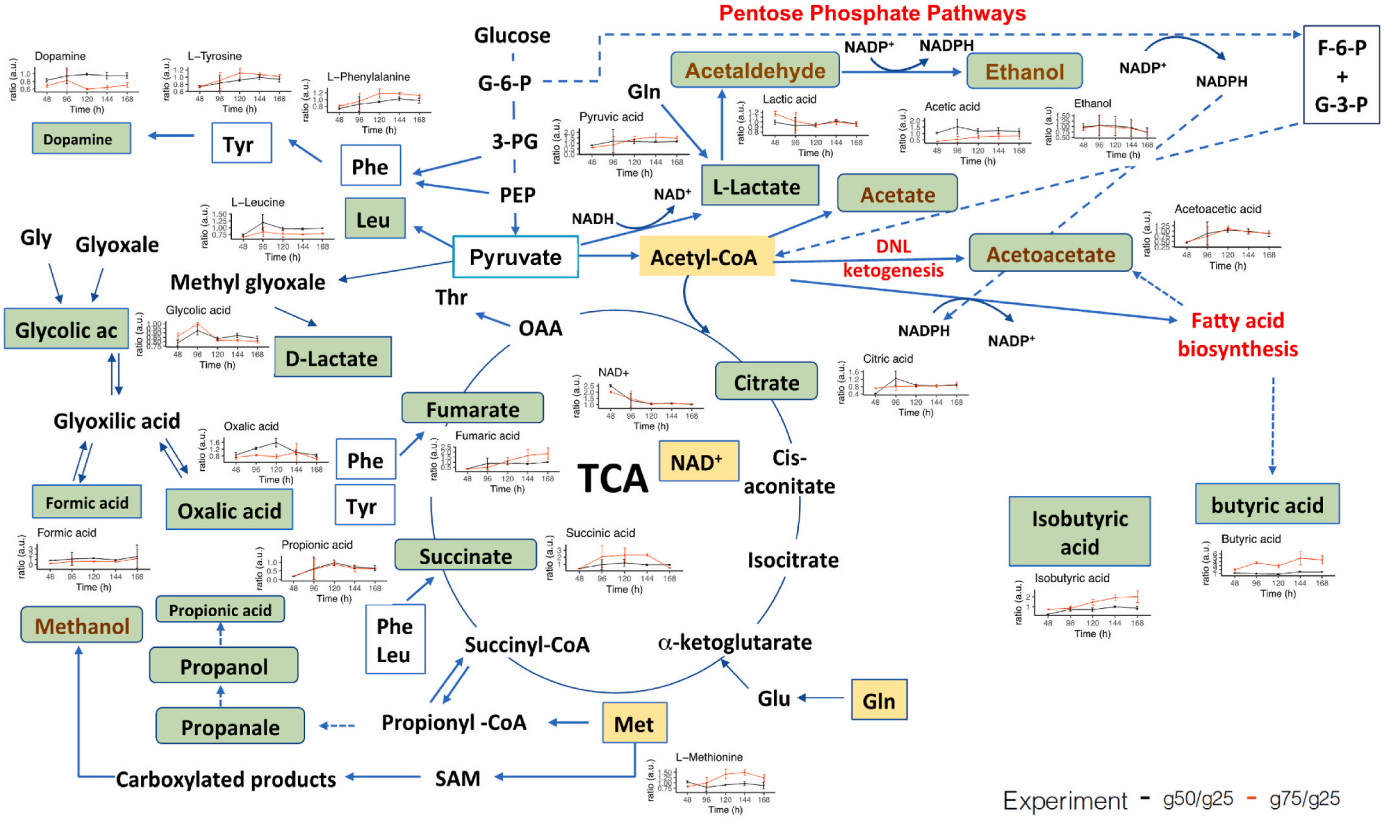

Fig. 7. Potential pathways involving the metabolites determined in CCM of HN9.10e cell lines, assuming specific or aspecific transport outside the cells [71,75,76,77–80]. Time resolved extracellular metabolite concentration in HN9.10e cell lines are reported as ratio for black: 50 mM glucose/25 mM glucose, red: 75 mM glucose/25 mM glucose. Error bars denote standard error of mean (SE). In our experiment the CCM was refreshed at each sampling time point, thus the measurement of metabolites variation is an indication of the activity and vitality of the cell for each specific time window. (For interpretation of the references to colour in this figure legend, the reader is referred to the Web version of this article.)

Dedication

This work is dedicated to the memory of Dr Laura Colombaioni who prematurely passed away in August 2021. Laura was an unsurpassed and professional colleague and friend.

Data availability statement

The data presented in this study are available in supplementary material.

CRediT authorship contribution statement

Laura Colombaioni: performed cell imaging by differential interference contrast microscopy, contributed toward design of the research, in interpretation of results, and in writing the paper. **Beatrice Campanella:** performed statistical analysis, contributed toward design of the research, in interpretation of results, and in writing the paper. **Riccardo Nieri:** performed HPLC-DAD analysis, contributed toward design of the research, in interpretation of results, and in writing the paper. **Massimo Onor:** prepared the samples and performed SPME-HS-GCMS analysis, contributed toward design of the research, in interpretation of results, and in writing the paper. **Edoardo Benedetti:** contributed toward design of the research, in interpretation of results, and in writing the paper. **Emilia Bramanti:** performed HPLC-DAD analysis, contributed toward design of the research, in interpretation of results, and in writing the paper.

Declaration of competing interest

The authors declare no conflict of interest.

Appendix A. Supplementary data

Supplementary data to this article can be found online at https://doi.org/10.1016/j.ab.2022.114607.

References

[1] P. Mergenthaler, U. Lindauer, G.A. Dienel, A. Meisel, Sugar for the brain: the role of glucose in physiological and pathological brain function, Trends Neurosci. 36 (2013) 587–597.
[2] N.R. Sibson, A. Dhankhar, G.F. Mason, D.L. Rothman, K.L. Behar, R.G. Shulman, Stoichiometric coupling of brain glucose metabolism and glutamatergic neuronal activity, Proc. Natl. Acad. Sci. Unit. States Am. 95 (1998) 316, https://doi.org/10.1073/pnas.95.1.316. LP – 321.
[3] C.W. Huang, C.C. Huang, J.T. Cheng, J.J. Tsai, S.N. Wu, Glucose and hippocampal neuronal excitability: role of ATP-sensitive potassium channels, J. Neurosci. Res. 85 (2007) 1468–1477, https://doi.org/10.1002/jnr.21284.
[4] A.A. Dunn-Meynell, N.E. Rawson, B.E. Levin, Distribution and phenotype of neurons containing the ATP-sensitive K+ channel in rat brain, Brain Res. 814 (1998) 41–54, https://doi.org/10.1016/S0006-8993(98)00956-1.
[5] S.J. Cho, K.A. Kang, M.J. Piao, Y.S. Ryu, P.D.S.M. Fernando, A.X. Zhen, Y.J. Hyun, M.J. Ahn, H.K. Kang, J.W. Hyun, 7,8-dihydroxyflavone protects high glucose-damaged neuronal cells against oxidative stress, Biomol. Ther. 27 (2019) 85–91, https://doi.org/10.4062/biomolther.2018.202.
[6] S.L. Macauley, M. Stanley, E.E. Caesar, S.A. Yamada, M.E. Raichle, R. Perez, T. E. Mahan, C.L. Sutphen, D.M. Holtzman, Hyperglycemia modulates extracellular amyloid-β concentrations and neuronal activity in vivo, J. Clin. Invest. 125 (2015) 2463–2467, https://doi.org/10.1172/JCI79742.
[7] D. Liu, H. Zhang, W. Gu, M. Zhang, Effects of exposure to high glucose on primary cultured hippocampal neurons: involvement of intracellular ROS accumulation, Neurol. Sci. 35 (2014) 831–837.
[8] J.W. Russel, G. David, A.M. Vincent, P.I.A. Mahendru, J.A. Olzmann, A. Mentzer, E. V.A.L. Feldman, High glucose-induced oxidative stress and mitochondrial dysfunction in neurons, Faseb. J. 16 (2002) 1738–1748.
[9] Y. Peng, J. Liu, L. Shi, Y. Tang, D. Gao, J. Long, J. Liu, Mitochondrial dysfunction precedes depression of AMPK/AKT signaling in insulin resistance induced by high glucose in primary cortical neurons, J. Neurochem. 137 (2016) 701–713.
[10] A.M. Stranahan, T. V Arumugam, R.G. Cutler, K. Lee, J.M. Egan, M.P. Mattson, Diabetes impairs hippocampal function through glucocorticoid-mediated effects on new and mature neurons, Nat. Neurosci. 11 (2008) 309–317.
[11] A.G. Dayer, K.M. Cleaver, T. Abouantoun, H.A. Cameron, New GABAergic interneurons in the adult neocortex and striatum are generated from different precursors, J. Cell Biol. 168 (2005) 415–427, https://doi.org/10.1083/jcb.200407053.
[12] E. Gould, A.J. Reeves, M.S.A. Graziano, C.G. Gross, Neurogenesis in the neocortex of adult primates, Science 286 (1999) 548–552, https://doi.org/10.1126/science.286.5439.548.
[13] J.T. Gonçalves, S.T. Schafer, F.H. Gage, Adult neurogenesis in the hippocampus: from stem cells to behavior, Cell 167 (2016) 897–914.
[14] W. Deng, J.B. Aimone, F.H. Gage, New neurons and new memories: how does adult hippocampal neurogenesis affect learning and memory? Nat. Rev. Neurosci. 11 (2010) 339–350, https://doi.org/10.1038/nrn2822.
[15] G. Kempermann, H.G. Kuhn, F.H. Gage, More hippocampal neurons in adult mice living in an enriched environment, Nature 386 (1997) 493–495, https://doi.org/10.1038/386493a0.
[16] S.C. Danzer, Depression, stress, epilepsy and adult neurogenesis, Exp. Neurol. 233 (2012) 22–32, https://doi.org/10.1016/j.expneurol.2011.05.023.
[17] D.M. Apple, R.S. Fonseca, E. Kokovay, The role of adult neurogenesis in psychiatric and cognitive disorders, Brain Res. 1655 (2017) 270–276, https://doi.org/10.1016/j.brainres.2016.01.023.
[18] N.K. Mule, J.N. Singh, Diabetes mellitus to neurodegenerative disorders: is oxidative stress fueling the flame? CNS Neurol. Disord. Targets (Formerly Curr. Drug Targets-CNS Neurol. Disord. 17 (2018) 644–653.
[19] T. Bartsch, P. Wulff, The hippocampus in aging and disease: from plasticity to vulnerability, Neuroscience 309 (2015) 1–16, https://doi.org/10.1016/j.neuroscience.2015.07.084.
[20] L. Zhao, M. Dong, D. Wang, M. Ren, Y. Zheng, H. Zheng, C. Li, H. Gao, Characteristic metabolic alterations identified in primary neurons under high glucose exposure, Front. Cell. Neurosci. 12 (2018), https://doi.org/10.3389/fncel.2018.00207.
[21] M.K. Aurich, G. Paglia, Ó. Rolfsson, S. Hrafnsdóttir, M. Magnúsdóttir, M. M. Stefaniak, B.Ø. Palsson, R.M.T. Fleming, I. Thiele, Prediction of intracellular metabolic states from extracellular metabolomic data, Metabolomics 11 (2015) 603–619, https://doi.org/10.1007/s11306-014-0721-3.
[22] T.M. Duarte, N. Carinhas, A.C. Silva, P.M. Alves, A.P. Teixeira, H-1-NMR protocol for exometabolome analysis of cultured mammalian cells, in: R. Portner (Ed.), Anim. CELL Biotechnol. METHODS Protoc, 3RD Ed., 2014, pp. 237–247, https://doi.org/10.1007/978-1-62703-733-4_16.
[23] C. Ferreiro-Vera, J.M. Mata-Granados, F. Priego-Capote, J.M. Quesada-Gomez, M. D.L. de Castro, Automated targeting analysis of eicosanoid inflammation biomarkers in human serum and in the exometabolome of stem cells by SPE-LC-MS/MS, Anal. Bioanal. Chem. 399 (2011) 1093–1103, https://doi.org/10.1007/s00216-010-4400-6.
[24] C.C. Marasco, J.R. Enders, K.T. Seale, J.A. McLean, J.P. Wikswo, Real-time cellular exometabolome analysis with a microfluidic-mass spectrometry platform, PLoS One 10 (2015), https://doi.org/10.1371/journal.pone.0117685.
[25] F.S. Amaro, J. Pinto, S. Rocha, A.M. Araujo, V.M. Goncalves, C. Jeronimo, R. Henrique, M.D.L. Bastos, M. Carvalho, P.G.D. Pinho, In vitro volatile exometabolome signature of clear cell renal cell carcinoma, MA, Toxicol. Lett. 350 (2021). S107–S107.
[26] J. Vappiani, T. Eyster, K. Orzechowski, D. Ritz, P. Patel, D. Sevin, J. Aon, Exometabolome profiling reveals activation of the carnitine buffering pathway in fed-batch cultures of CHO cells co-fed with glucose and lactic acid, Biotechnol. Prog.. (n.d.). doi:10.1002/btpr.3198..
[27] Z. León, J.C. García-Cañaveras, M.T. Donato, A. Lahoz, Mammalian cell metabolomics: experimental design and sample preparation, Electrophoresis 34 (2013) 2762–2775, https://doi.org/10.1002/elps.201200605.
[28] M. Wright Muelas, F. Ortega, R. Breitling, C. Bendtsen, H.V. Westerhoff, Rational cell culture optimization enhances experimental reproducibility in cancer cells, Sci. Rep. 8 (2018) 3029, https://doi.org/10.1038/s41598-018-21050-4.
[29] L. Colombaioni, M. Onor, E. Benedetti, E. Bramanti, Thallium stimulates ethanol production in immortalized hippocampal neurons, PLoS One 12 (2017), e0188351, https://doi.org/10.1371/journal.pone.0188351.
[30] E. Bramanti, M. Onor, L. Colombaioni, Neurotoxicity induced by low thallium doses in living hippocampal neurons: evidence of early onset mitochondrial dysfunction and correlation with ethanol production, ACS Chem. Neurosci. (2019), https://doi.org/10.1021/acschemneuro.8b00343.
[31] B. Campanella, L. Colombaioni, R. Nieri, E. Benedetti, M. Onor, E. Bramanti, Unraveling the extracellular metabolism of immortalized hippocampal neurons under normal growth conditions, Front. Chem. 9 (2021) 132, https://doi.org/10.3389/fchem.2021.621548.
[32] L. Colombaioni, L.M. Frago, I. Varela-Nieto, R. Pesi, M. Garcia-Gil, Serum deprivation increases ceramide levels and induces apoptosis in undifferentiated HN9.10e cells, Neurochem. Int. 40 (2002) 327–336, https://doi.org/10.1016/s0197-0186(01)00090-0.
[33] H.J. Lee, D.N. Hammond, T.H. Large, J.D. Roback, J.A. Sim, D.A. Brown, U. H. Otten, B.H. Wainer, Neuronal properties and trophic activities of immortalized hippocampal cells from embryonic and young adult mice, J. Neurosci. 10 (1990) 1779–1787. http://www.ncbi.nlm.nih.gov/pubmed/2113086. (Accessed 31 May 2021).
[34] L. Colombaioni, L.M. Frago, I. Varela-Nieto, R. Pesi, M. Garcia-Gil, Serum deprivation increases ceramide levels and induces apoptosis in undifferentiated HN9.10e cells, Neurochem. Int. 40 (2002) 327–336, https://doi.org/10.1016/s0197-0186(01)00090-0.
[35] S. Rello, J.C. Stockert, V. Moreno, A. Gámez, M. Pacheco, A. Juarranz, M. Cañete, A. Villanueva, A. Gámez, M. Pacheco, A. Juarranz, M. Cañete, A. Villanueva, Morphological criteria to distinguish cell death induced by apoptotic and necrotic

treatments, Apoptosis 10 (2005) 201–208, https://doi.org/10.1007/s10495-005-6075-6.
[36] R. Leardi, Chemometrics in data analysis, Chromatogr. Anal. Environ. (2006) 221–241.
[37] M. Wallace, H. Whelan, L. Brennan, Metabolomic analysis of pancreatic beta cells following exposure to high glucose, Biochim. Biophys. Acta Gen. Subj. 1830 (2013) 2583–2590.
[38] J.K. Meissen, K.M. Hirahatake, S.H. Adams, O. Fiehn, Temporal metabolomic responses of cultured HepG2 liver cells to high fructose and high glucose exposures, Metabolomics 11 (2015) 707–721.
[39] S. Bernardo-Bermejo, E. Sánchez-López, M. Castro-Puyana, S. Benito-Martínez, F. J. Lucio-Cazaña, M.L. Marina, A non-targeted capillary electrophoresis-mass spectrometry strategy to study metabolic differences in an in vitro model of high-glucose induced changes in human proximal tubular HK-2 cells, Molecules 25 (2020) 512.
[40] S. Bernardo-Bermejo, E. Sánchez-López, M. Castro-Puyana, S. Benito, F.J. Lucio-Cazaña, M.L. Marina, An untargeted metabolomic strategy based on liquid chromatography-mass spectrometry to study high glucose-induced changes in HK-2 cells, J. Chromatogr., A 1596 (2019) 124–133.
[41] P.Z. Wei, W.W.-S. Fung, J.K.-C. Ng, K.-B. Lai, C.C.-W. Luk, K.M. Chow, P.K.-T. Li, C. C. Szeto, Metabolomic changes of Human proximal tubular cell Line in High Glucose environment, Sci. Rep. 9 (2019) 1–7.
[42] R. Gruetter, E.J. Novotny, S.D. Boulware, D.L. Rothman, G.F. Mason, G.I. Shulman, R.G. Shulman, W. V Tamborlane, Direct measurement of brain glucose concentrations in humans by 13C NMR spectroscopy, Proc. Natl. Acad. Sci. U.S.A. 89 (1992) 1109–1112, https://doi.org/10.1073/pnas.89.3.1109.
[43] Y. Huang, Z.-G. Xiong, Choosing an appropriate glucose concentration according to different cell types and experimental purposes is very important, Cell Stress Chaperones 20 (2015) 1–2, https://doi.org/10.1007/s12192-014-0547-y.
[44] A. Ronowska, A. Szutowicz, H. Bielarczyk, S. Gul-Hinc, J. Klimaszewska-Łata, A. Dyś, M. Zyśk, A. Jankowska-Kulawy, The regulatory effects of acetyl-CoA distribution in the healthy and diseased brain, Front. Cell. Neurosci. 12 (2018) 169, https://doi.org/10.3389/fncel.2018.00169.
[45] R.J. Reiter, R. Sharma, Q. Ma, S. Rorsales-Corral, L.G. de Almeida Chuffa, Melatonin inhibits Warburg-dependent cancer by redirecting glucose oxidation to the mitochondria: a mechanistic hypothesis, Cell. Mol. Life Sci. 77 (2020) 2527–2542, https://doi.org/10.1007/s00018-019-03438-1.
[46] R.-H. Yang, J. Lin, X.-H. Hou, R. Cao, F. Yu, H.-Q. Liu, A.-L. Ji, X.-N. Xu, L. Zhang, F. Wang, Effect OF docosahexaenoic acid ON hippocampal neurons IN high-glucose condition: INVOLVEMENT OF PI3K/AKT/NUCLEAR FACTOR-kappa B-MEDIATED INFLAMMATORY PATHWAYS, Neuroscience 274 (2014) 218–228, https://doi.org/10.1016/j.neuroscience.2014.05.042.
[47] H. Wang, J. Deng, L. Chen, K. Ding, Y. Wang, Acute glucose fluctuation induces inflammation and neurons apoptosis in hippocampal tissues of diabetic rats, J. Cell. Biochem. (n.d.). doi:10.1002/jcb.29523.
[48] S.R. Oliveira, J.D. Amaral, C.M.P. Rodrigues, Mechanism and disease implications of necroptosis and neuronal inflammation, Cell Death Dis. 9 (2018) 903, https://doi.org/10.1038/s41419-018-0872-7.
[49] K. Pierre, L. Pellerin, Monocarboxylate transporters, Encycl. Neurosci. (2009) 961–965, https://doi.org/10.1016/B978-008045046-9.01714-9.
[50] K. Brauburger, G. Burckhardt, B.C. Burckhardt, The sodium-dependent di- and tricarboxylate transporter, NaCT, is not responsible for the uptake of D-, L-2-hydroxyglutarate and 3-hydroxyglutarate into neurons, J. Inherit. Metab. Dis. 34 (2011) 477–482, https://doi.org/10.1007/s10545-010-9268-2.
[51] V. Gogvadze, B. Zhivotovsky, S. Orrenius, The Warburg effect and mitochondrial stability in cancer cells, Mol. Aspect. Med. 31 (2010) 60–74, https://doi.org/10.1016/j.mam.2009.12.004.
[52] C.E. Hanzel, S.V. Verstraeten, Thallium induces hydrogen peroxide generation by impairing mitochondrial function, Toxicol. Appl. Pharmacol. 216 (2006) 485–492, https://doi.org/10.1016/j.taap.2006.07.003.
[53] A.G. Antoshechkin, On intracellular formation of ethanol and its possible role in energy metabolism, Alcohol Alcohol 36 (2001) 608, https://doi.org/10.1093/alcalc/36.6.608.
[54] R.A. Gatenby, R.J. Gillies, Why do cancers have high aerobic glycolysis? Nat. Rev. Cancer 4 (2004) 891–899, https://doi.org/10.1038/nrc1478.
[55] A. van Waarde, G. Van den Thillart, M. Verhagen, Ethanol Formation and pH-Regulation in Fish, CRC Press, Boca Raton, 1993, pp. 157–170.
[56] Y.L. Dorokhov, A.V. Shindyapina, E.V. Sheshukova, T.V. Komarova, Metabolic methanol: molecular pathways and physiological roles, Physiol. Rev. 95 (2015) 603–644, https://doi.org/10.1152/physrev.00034.2014.
[57] H. Riveros-Rosas, A. Julian-Sanchez, E. Pinã, Enzymology of ethanol and acetaldehyde metabolism in mammals, Arch. Med. Res. 28 (1997) 453–471.
[58] D. Liu, M. Pitta, M.P. Mattson, Preventing NAD(+) depletion protects neurons against excitotoxicity: bioenergetic effects of mild mitochondrial uncoupling and caloric restriction, Ann. N. Y. Acad. Sci. 1147 (2008) 275–282, https://doi.org/10.1196/annals.1427.028.
[59] Y. Aman, Y. Qiu, J. Tao, E.F. Fang, Therapeutic potential of boosting NAD+ in aging and age-related diseases, Transl. Med. Aging. 2 (2018) 30–37, https://doi.org/10.1016/j.tma.2018.08.003.
[60] J. Yoshino, J.A. Baur, S. Imai, NAD+ intermediates: the biology and therapeutic potential of NMN and NR, Cell Metabol. 27 (2018) 513–528, https://doi.org/10.1016/j.cmet.2017.11.002.
[61] Y. Hou, S. Lautrup, S. Cordonnier, Y. Wang, D.L. Croteau, E. Zavala, Y. Zhang, K. Moritoh, J.F. O'Connell, B.A. Baptiste, T. V Stevnsner, M.P. Mattson, V.A. Bohr, NAD(+) supplementation normalizes key Alzheimer's features and DNA damage responses in a new AD mouse model with introduced DNA repair deficiency, Proc. Natl. Acad. Sci. U.S.A. 115 (2018) E1876, https://doi.org/10.1073/pnas.1718819115. –E1885.
[62] E. Katsyuba, M. Romani, D. Hofer, J. Auwerx, NAD+ homeostasis in health and disease, Nat. Metab. 2 (2020) 9–31, https://doi.org/10.1038/s42255-019-0161-5.
[63] D. Liu, S.L. Chan, N.C. de Souza-Pinto, J.R. Slevin, R.P. Wersto, M. Zhan, K. Mustafa, R. de Cabo, M.P. Mattson, Mitochondrial UCP4 mediates an adaptive shift in energy metabolism and increases the resistance of neurons to metabolic and oxidative stress, NeuroMolecular Med. 8 (2006) 389–414, https://doi.org/10.1385/NMM:8:3:389.
[64] M.E. Cueno, N. Kamio, K. Seki, T. Kurita-Ochiai, K. Ochiai, High butyric acid amounts induce oxidative stress, alter calcium homeostasis, and cause neurite retraction in nerve growth factor-treated PC12 cells, Cell Stress Chaperones 20 (2015) 709–713, https://doi.org/10.1007/s12192-015-0584-1.
[65] M.A. Cayo, A.K. Cayo, S.M. Jarjour, H. Chen, Sodium butyrate activates Notch1 signaling, reduces tumor markers, and induces cell cycle arrest and apoptosis in pheochromocytoma, Am. J. Transl. Res. 1 (2009) 178–183. https://pubmed.ncbi.nlm.nih.gov/19956429.
[66] B.B. Nankova, R. Agarwal, D.F. MacFabe, E.F. La Gamma, Enteric bacterial metabolites propionic and butyric acid modulate gene expression, including CREB-dependent catecholaminergic neurotransmission, in PC12 cells - possible relevance to autism spectrum disorders, PLoS One 9 (2014), e103740, https://doi.org/10.1371/journal.pone.0103740.
[67] D.L. Nelson, M.M. Cox, A.L. Lehninger, Principles of Biochemistry, fourth ed. Ed, vol. 1, WH Free. Company, New York, 2005, p. 2.
[68] W.H. Freeman, S. Learning, in: Principles of Biochemistry, Seventh, macmillan learning, 2017.
[69] A. Herrero-Mendez, A. Almeida, E. Fernández, C. Maestre, S. Moncada, J. P. Bolaños, The bioenergetic and antioxidant status of neurons is controlled by continuous degradation of a key glycolytic enzyme by APC/C–Cdh1, Nat. Cell Biol. 11 (2009) 747–752, https://doi.org/10.1038/ncb1881.
[70] J.P. Bolaños, A. Almeida, S. Moncada, Glycolysis: a bioenergetic or a survival pathway? Trends Biochem. Sci. 35 (2010) 145–149, https://doi.org/10.1016/j.tibs.2009.10.006.
[71] Z. Nochi, R.K.J. Olsen, N. Gregersen, Short-chain acyl-CoA dehydrogenase deficiency: from gene to cell pathology and possible disease mechanisms, J. Inherit. Metab. Dis. 40 (2017) 641–655, https://doi.org/10.1007/s10545-017-0047-1.
[72] J.S. Chen, D. V Faller, R.A. Spanjaard, Short-chain fatty acid inhibitors of histone deacetylases: promising anticancer therapeutics? Curr. Cancer Drug Targets 3 (2003) 219–236, https://doi.org/10.2174/1568009033481994.
[73] R. Graber, C. Sumida, E.A. Nunez, Fatty acids and cell signal transduction, J. Lipid Mediat. Cell Signal 9 (1994) 91–116.
[74] M.W. Gray, G. Burger, B.F. Lang, Mitochondrial evolution, Science 283 (1999) 1476–1481, 84.
[75] B. Polis, A.O. Samson, Role of the metabolism of branched-chain amino acids in the development of Alzheimer's disease and other metabolic disorders, Neural Regen. Res. 15 (2020) 1460–1470, https://doi.org/10.4103/1673-5374.274328.
[76] N. Heeley, P. Kirwan, T. Darwish, M. Arnaud, M.L. Evans, F.T. Merkle, F. Reimann, F.M. Gribble, C. Blouet, Rapid sensing of l-leucine by human and murine hypothalamic neurons: neurochemical and mechanistic insights, Mol. Metabol. 10 (2018) 14–27, https://doi.org/10.1016/j.molmet.2018.01.021.
[77] A.S. Divakaruni, M. Wallace, C. Buren, K. Martyniuk, A.Y. Andreyev, E. Li, J. A. Fields, T. Cordes, I.J. Reynolds, B.L. Bloodgood, L.A. Raymond, C.M. Metallo, A. N. Murphy, Inhibition of the mitochondrial pyruvate carrier protects from excitotoxic neuronal death, J. Cell Biol. 216 (2017) 1091–1105, https://doi.org/10.1083/jcb.201612067.
[78] D.S. Wishart, Y.D. Feunang, A. Marcu, A.C. Guo, K. Liang, R. Vazquez-Fresno, T. Sajed, D. Johnson, C. Li, N. Karu, Z. Sayeeda, E. Lo, N. Assempour, M. Berjanskii, S. Singhal, D. Arndt, Y. Liang, H. Badran, J. Grant, A. Serra-Cayuela, Y. Liu, R. Mandal, V. Neveu, A. Pon, C. Knox, M. Wilson, C. Manach, A. Scalbert, Hmdb 4.0: the human metabolome database for 2018, Nucleic Acids Res. 46 (2018) D608–D617, https://doi.org/10.1093/nar/gkx1089.
[79] E. Meléndez-Hevia, P. De Paz-Lugo, A. Cornish-Bowden, M.L. Cárdenas, A weak link in metabolism: the metabolic capacity for glycine biosynthesis does not satisfy the need for collagen synthesis, J. Bio. Sci. 34 (2009) 853–872, https://doi.org/10.1007/s12038-009-0100-9.
[80] Y. Toyoda, C. Erkut, F. Pan-Montojo, S. Boland, M.P. Stewart, D.J. Mueller, W. Wurst, A.A. Hyman, T. V Kurzchalia, Products of the Parkinson's disease-related glyoxalase DJ-1, D-lactate and glycolate, support mitochondrial membrane potential and neuronal survival, Biol. Open. 3 (2014) 777–784, https://doi.org/10.1242/bio.20149399.
[81] C.G. McNamara, Á. Tejero-Cantero, S. Trouche, N. Campo-Urriza, D. Dupret, Dopaminergic neurons promote hippocampal reactivation and spatial memory persistence, Nat. Neurosci. 17 (2014) 1658–1660, https://doi.org/10.1038/nn.3843.
[82] J.P. Ruddick, A.K. Evans, D.J. Nutt, S.L. Lightman, G.A.W. Rook, C.A. Lowry, Tryptophan metabolism in the central nervous system: medical implications, Expet Rev. Mol. Med. 8 (2006) 1–27, https://doi.org/10.1017/S1462399406000068.
[83] E. Höglund, Ø. Øverli, S. Winberg, Tryptophan metabolic pathways and brain serotonergic activity: a comparative review, Front. Endocrinol. 10 (2019) 158, https://doi.org/10.3389/fendo.2019.00158.
[84] S.M. Hutson, E. Lieth, K.F. LaNoue, Function of leucine in excitatory neurotransmitter metabolism in the central nervous system, J. Nutr. 131 (2001) 846S–850S, https://doi.org/10.1093/jn/131.3.846S.
[85] L. Massieu, M.L. Haces, T. Montiel, K. Hernández-Fonseca, Acetoacetate protects hippocampal neurons against glutamate-mediated neuronal damage during

glycolysis inhibition, Neuroscience 120 (2003) 365–378, https://doi.org/10.1016/s0306-4522(03)00266-5.

[86] H.S. Noh, Y.-S. Hah, R. Nilufar, J. Han, J.-H. Bong, S.S. Kang, G.J. Cho, W.S. Choi, Acetoacetate protects neuronal cells from oxidative glutamate toxicity, J. Neurosci. Res. 83 (2006) 702–709, https://doi.org/10.1002/jnr.20736.

[87] M. Wu, A. Neilson, A.L. Swift, R. Moran, J. Tamagnine, D. Parslow, S. Armistead, K. Lemire, J. Orrell, J. Teich, S. Chomicz, D.A. Ferrick, Multiparameter metabolic analysis reveals a close link between attenuated mitochondrial bioenergetic function and enhanced glycolysis dependency in human tumor cells, Am. J. Physiol. Cell Physiol. 292 (2007) C125–C136, https://doi.org/10.1152/ajpcell.00247.2006.